Synthesis and Electrochemical Properties of New C_{60}-Acceptor and -Donor Dyads

Michael Diekers[a], Andreas Hirsch*[a], Soomi Pyo[b], José Rivera[c], and Luis Echegoyen*[b]

Institut für Organische Chemie[a],
Henkestraße 42, D-91054 Erlangen, Germany

Department of Chemistry, University of Miami[b],
Coral Gables, FL 33124, USA

Department of Chemistry, Pontifical Catholic University[c],
Ponce, Puerto Rico 00732

Received December 11, 1997

Keywords: Cyclic voltammetry / Donor-acceptor systems / EPR spectroscopy / Fullerenes

The synthesis of new C_{60}-acceptor and C_{60}-donor dyads **6**–**8** by facile and irreversible [4+2]cycloadditions of anthraquinone- and anthraquinodimethane-based dienes with C_{60}, as well as by direct oxidative amination of C_{60} with *N,N′*-dimethyl-*o*-phenylenediamine is described. The complete electrochemical characterization and ESR-spectroscopic data of the C_{60}-acceptor dyads allows an unambiguous assignment of the location of each reduction step to one or other of the electroactive groups. The locations of the first oxidation and reduction events in all type A and -B systems investigated in this study correspond to the PM3-calculated HOMOs of the neutral species or the SOMOs of the singly reduced species. Whereas the anthraquinone moiety in **6** is a weaker acceptor than C_{60} , the introduction of the more electron-withdrawing cyanoimino groups at the 9,10-positions of the anthracene unit in the dyad **7** causes the first reduction to take place on the addend. This experimental and computational study has shown that both the C_{60}-acceptor dyad **7** and the C_{60}-donor dyad **8** are suitable precursors for the synthesis of the proposed type-D triads, which contain both a donor and an acceptor building block attached to the fullerene core in a stereochemically defined arrangement.

Introduction

Buckminsterfullerene C_{60} and its derivatives[1][2][3] exhibit a number of characteristic electronic and photophysical properties, which make them promising candidates for the investigation of light-induced electron-transfer processes and long-lived charge-separated states. For this purpose, a molecular architecture is required in which at least one additional chromophore or redox-active center is located in close proximity to the fullerene itself. The relative orientation as well as the distance between the chromophores determines the energy- and charge-transfer properties of such artificial models of photosynthetic systems. A suitable way of controlling the geometric arrangement of the individual building blocks is to covalently link them with rigid spacer units. To date, three types of dyads and triads (types A–C) involving a C_{60} moiety have been developed (Figure 1):

The remarkable acceptor properties of C_{60}, especially its ability to undergo up to six reversible one-electron reductions,[4] come to the fore in the design of fullerene-donor dyads (type A). A variety of donor molecules including porphyrins,[5][6][7][8][9][10][11][12] aromatic amines,[13][14][15] polycyclic aromatics,[16][17] transition-metal complexes,[18] carotenoids,[19] ferrocenes,[20][21][22] phthalocyanines,[23] hemiporphyrazines[24] as well as tetrathiafulvalenes[25] have been covalently attached to C_{60}. Whereas a charge-transfer from the donor to the fullerene in the ground state has not yet

Figure 1. Schematic representation of dyads and triads involving the C_{60} electrophore: A) C_{60}-donor, B) C_{60}-acceptor, C) C_{60}-donor^1-donor^2 (monoadduct with respect to C_{60}) and D) C_{60}-donor-acceptor (bisadduct with respect to C_{60})

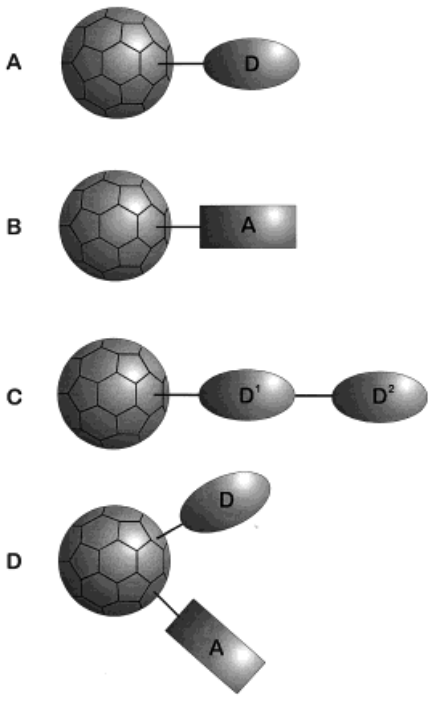

  1434–193X/98/0606–1111 $ 17.50+.50/0

been observed, several remarkable photoinduced electron-transfer phenomena have been studied in detail. For example, Imahori et al. showed that the fullerene moiety in C_{60}-porphyrin dyads causes an acceleration of the charge separation and a retardation of the charge recombination, compared to the rates for other acceptors with a redox potential similar to that of a benzoquinone derivative.[10] A long-lived charge-separated state of 250 ns was observed by Williams et al. in the case of a C_{60}-dimethylaniline dyad.[15] To date, only a few examples of C_{60}-acceptor dyads (type B) have been reported.[26][27][28][29][30][31][32] Since C_{60} itself is already very electronegative, the choice of suitable electroactive groups is restricted to very strong acceptors such as quinone, DCNQI and TCNQ derivatives. Cyclic voltammetric investigations of some of these dyads suggest that the first reduction step takes place at the acceptor.[26][27][28][29][30][31][32] However, since the difference between the first reduction potential of a quinone-acceptor and that of the fullerene moiety is small, only type B models involving strong acceptors such as TCNQ or DCNQI derivatives represent promising models for effective charge-separation processes. Better model systems should allow for charge separation in several successive steps, akin to the situation in natural photosynthetic events. The first example of such a complex system involving a fullerene electroactive group is a type C triad (Figure 1) containing two donors, namely a carotene and a porphyrin subunit.[33] Some of the photophysical properties of this triad are reminiscent of those observed in natural photosynthesis. In the present paper, we propose new triads of type D (Figure 1), in which the C_{60} moiety is not located at the periphery of the molecular array but serves as a central building block linking the donor and the acceptor. This concept has the advantage that the geometric arrangement of the three electrophores can be systematically varied over a wide range, since at least nine different regioisomers can be formed from successive additions to [6,6]-bonds (Figure 2).

Figure 2. Positional relationships of the double bonds in a C_{60} monoadduct relative to the [6,6]-bond (bold) carrying the first addend

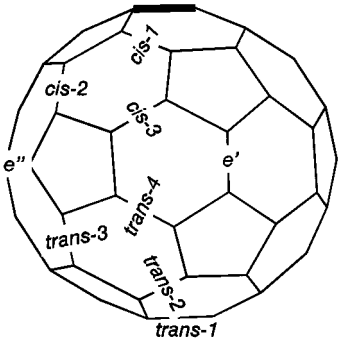

Recently, we have carried out extensive investigations into the regiochemistry of multiple additions to C_{60} and have discovered several regioselectivity principles. These findings form a basis for the design of type-D systems.[34] Another advantage of this type of triads is that the addition pattern itself also influences the electronic properties of the fullerene core. For example, different regioisomers of bisadducts give rise to different electronic absorption spectra.[1][2]

En route to type-D triads such as **1**, we report in this paper on the synthesis and characterization of C_{60}-acceptor and -donor subunits of types A and B. We provide the first complete electrochemical characterization of C_{60}-acceptor dyads as well as some ESR spectroscopic data, allowing an unambiguous assignment of the location of each reduction step to one or other of the electrophores. The locations of the first oxidation and reduction events in all type A and B systems investigated in this study correspond to the PM3-calculated HOMOs of the neutral species or the SOMOs of the singly reduced species.

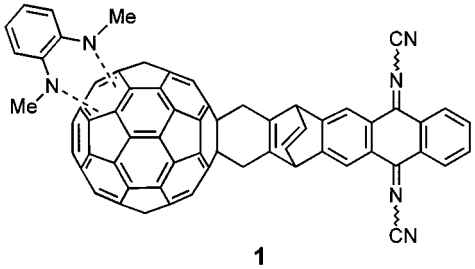

1

Results and Discussion

Synthesis and Characterization: A precursor-acceptor building block for a type B dyad has to fulfil three important requirements: (i) It has to contain a functional group allowing for a facile addition to C_{60} in good yields, (ii) the linkage between the redox-active centers should be rigid, and (iii) the reduction potential of the acceptor must be more positive than that of C_{60}. We therefore decided to use DCNQI acceptors[35][36] with a fused dieno moiety, which can be expected to readily undergo a [4+2] cycloaddition with a [6,6]-double bond of C_{60}.

As a versatile precursor system for the introduction of a dieno moiety into an acceptor system, we decided to use Vogels′ bis-diene,[37] **2**, which is readily available in five steps from commercially available starting materials.[38] Bis-dienes of this type are very attractive starting materials for the preparation of polycyclic, polyfunctional systems by means of successive Diels-Alder additions. Specifically, the enophilicity of the dieno moiety in a monoadduct of **2**, which is considerably reduced compared to that of the parent compound, allows for a good chemoselectivity. As starting material for the acceptor moiety we used naphthoquinone (Scheme 1) because, in contrast to benzoquinones, it contains only one reactive double bond. The [4+2] cycloaddition of **2** with naphthoquinone afforded the tetrahydroanthraquinone, **3**, which was subsequently oxidized to the anthraquinone **4** by treatment with KOH in air. The overall isolated yield of **4** was 65%. Knoevenagel condensation of **4** with bis(trimethylsilyl)carbodiimide in the presence of titanium tetrachloride (Lehnerts reagent)[35][39] furnished the corresponding *N*,*N*′-dicyanoquinonediimine **5** in 48% yield. Subsequent Diels-Alder reactions of **4** and **5**

with C_{60} afforded **6** and **7** in 49% and 42% yield, respectively (Scheme 1).

Scheme 1

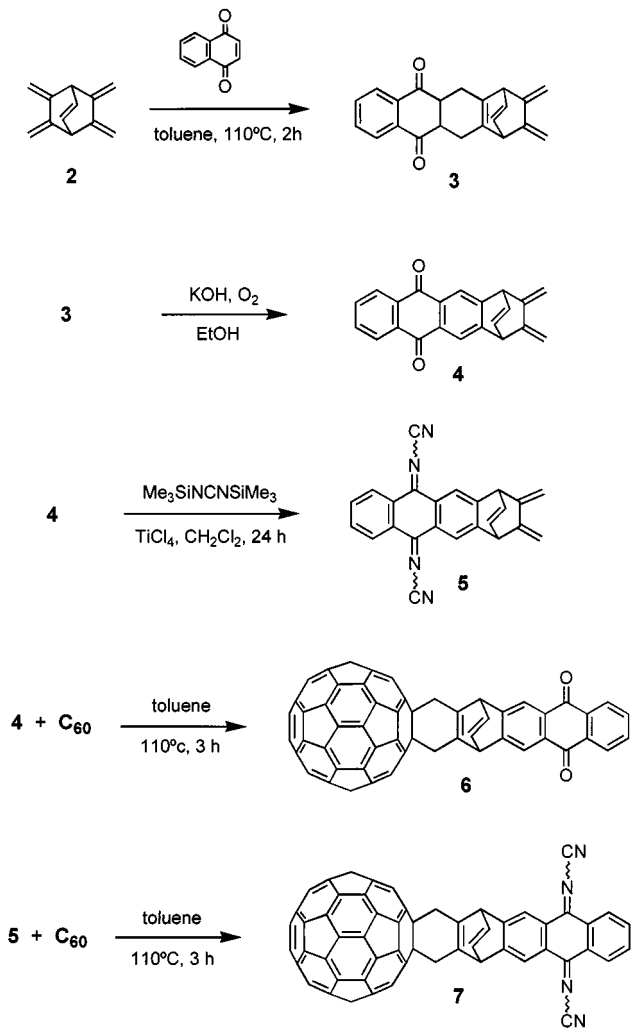

The complete spectroscopic characterization of the dienes **3**, **4** and **5** and of the monoadducts **6** and **7** was achieved by NMR, UV/Vis and FT-IR spectroscopy, as well as by mass spectrometry. The ^{13}C-NMR spectrum of **3** displays 11 signals, as would be expected in view of its C_s symmetry. The carbonyl C atoms resonate at $\delta = 197.6$. The ^{13}C-NMR spectrum of anthraquinone **4** is similar to that of **3**. The signal of the carbonyl C atoms is slightly highfield shifted, as would be expected for a quinoid system, and appears at $\delta = 183.2$. Nine signals appear in the sp^2 region between $\delta = 105$ and 149. The signals for the bridgehead CH groups appear at $\delta = 51.9$. Characteristic features in the ^{1}H-NMR spectra of **3**–**5** are two singlets for the protons of the olefinic CH_2 groups within the diene moiety, which in the case of **4** appear at $\delta = 5.11$ and 5.30. The ^{1}H-NMR spectrum of **5** shows a strong, broad signal at $\delta = 8.7$, which is due to the four aromatic protons located in the vicinity of the cyanoimino groups. This broadening is a known phenomenon[34] and is due to a *syn-anti* isomerization. The ^{13}C-NMR spectrum of **5** displays only 10 signals instead of 12, again in line with expectation given the depicted symmetry. The C atoms of the cyano groups resonate at $\delta = 113.8$ and those of the imino groups at $\delta = 171.6$. The FT-IR spectrum of **5** shows a characteristic cyano band at 2161 cm^{-1}. The NMR and UV/Vis spectra of **6** and **7** are typical of those of monoadducts of C_{60}. The ^{13}C-NMR spectra of **6** and **7** each show 31 signals for fullerene C atoms in the sp^2 region and one signal at $\delta = 66.95$ for the sp^3 C atom of the C_{60} core, as expected in view of the C_S symmetry of the monoadduct. The UV/Vis spectra of the monoadducts **6** and **7** show the typical absorption for closed [6,6]-bridged monoadducts at 434 nm. In the ^{1}H-NMR spectra of **6** and **7**, the signals of the two methylene groups generated during the Diels-Alder reaction appear at $\delta = 4.3$. The MALDI/TOF or FAB mass-spectra show the M^+ peaks of the monoadducts **6** and **7** together with several fragmentation peaks.

In order to develop a new C_{60}-donor dyad, we took advantage of the direct addition of amines accompanied by oxidative dehydrogenation. This type of reaction is known to work well with secondary aliphatic amines.[40] If diamines are used, the corresponding dehydrogenated [6,6] monoadducts are obtained in moderate to good yields. In order to introduce an electrophore by this type of reaction, we decided to use for the first time an aromatic diamine, namely *N*,*N*′-dimethyl-*o*-phenylenediamine (Scheme 2), which is readily available from *o*-phenylenediamine in three steps.[41] The lower basicity of aromatic amines should make them less reactive in this process than aliphatic amines, which was indeed borne out by experiment. A 20-% conversion to the monoadduct **8** required the use of a large excess of diamine and a reaction time of 14 days (Scheme 2).

Scheme 2

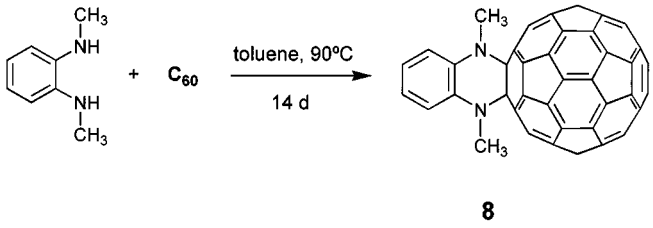

The ^{13}C-NMR spectrum of **8** displays 16 signals for C_{60} C-atoms and one signal for the two quaternary carbons of the aromatic ring of the addend in the sp^2 region. Some of the C_{60} sp^2-signals are slightly broadened, which is due to a slow exchange equilibrium of the two boat conformers. Furthermore, the spectrum shows the signals of the aromatic CH groups at $\delta = 122.4$ and 115.4. In the aliphatic region, the two expected signals attributable to the methyl groups and the sp^3 C-atoms of the fullerene core appear at $\delta = 37.28$ and 86.02. The ^{1}H-NMR spectrum shows one singlet for the methyl protons at $\delta = 3.78$ and, surprisingly, only one singlet for the four protons of the phenylene ring. In the FAB-MS spectrum of **8** the M^+ peak appears at $m/z = 854$.

Electrochemistry: Compounds **4**–**8** were studied electrochemically using a glassy carbon electrode in toluene/aceto-

nitrile (85:15) and after pumping the frozen solvent under high vacuum (10^{-6} Torr). In all cases, well resolved, reversible, and well behaved cyclic voltammetric waves were observed. Figure 3 shows the cyclic voltammograms of compounds **4** and **6**, recorded under essentially identical conditions, both referenced to internally added ferrocene. Compound **6** shows an initial reduction process at −1.12 V vs. Fc/Fc^+, much more positive than the first reduction process for compound **4**, which occurs at −1.44 V. Although anthraquinone is normally regarded as a good acceptor compound, **4** is found to be 320 mV more difficult to reduce than **6**. This situation is somewhat different from that previously reported for other fullerene-acceptor dyads, which typically exhibit a first reduction process that can be assigned to the acceptor adduct.[26][27][28][29][30][31][32] All electrochemical potentials are summarized in Table 1. Upon simple inspection of the cathodic and anodic currents in Figure 3, it is apparent that the second reduction step for **6** involves more than one electron. Although it is not possible to assert the exact number of electrons involved in this second reduction step based simply on the cyclic voltammetric data shown in Figure 3, it seems likely that it corresponds to two. Coulometric reductions confirmed these observations. This is consistent with the fact that the first reduction process for compound **4** occurs at −1.44 V, while the second reduction for **6** occurs at −1.48 V. Consequently, the second reduction step most likely involves an anthraquinone-based reduction, which is very close to the second reduction of the fullerene moiety. Such an interpretation would imply that the first reduction of **6** is fullerene-based, while the second involves a two-electron process, consisting of one fullerene-based and one anthraquinone-based reduction, resulting in the overall formation of the trianion of **6**. The separation between these reduction processes of **6** (360 mV) is consistent with the typically observed separation between successive reductions of fullerene derivatives.[42]

Table 1. $E_{1/2}$ values measured as the average of the anodic and cathodic peak potentials vs. the potential for the redox couple of internally added Fc/Fc^+. All couples were quasi-reversible with ΔE_{pp} values in the range 60−85 mV. The subscripts used with the potentials (E_i's) have no special significance other than to group corresponding processes for related compounds

Compound	E_1	E_2	E_3	E_4	E_5	E_6
C_{60}		−0.99	−1.39	−1.90	−2.37	−2.87
6		−1.12	−1.48	−2.06	−2.56	
4			−1.44	−1.97		
7	−0.78	−1.13	−1.52	−2.09	−2.48	
5	−0.80	−1.14				
8	+0.49*	−1.06	−1.46	−1.99		

* Oxidation potential.

Further inspection of Figure 3 reveals a third reduction process for **6**, which again is clearly composed of two very close waves that are impossible to resolve completely. Only the average potential of these two processes, −2.06 V, is reported in Table 1. This value is reasonably close to that observed for the second reduction of the model compound, **4**, which occurs at −1.97 V. It also corresponds well to the expected third reduction of a fullerene derivative, since it is 580 mV more negative than the previous one. It therefore seems likely that after these two closely spaced waves around −2.06 V, compound **6** is converted into its corresponding pentaanion. The close correspondence between the potentials of the second and third reductions of **6** and those of the first and second reductions of **4** is strong evidence for the formation of a pentaanion, one with three electrons mainly localized on the C_{60} moiety, and with two on the anthraquinone group. A fifth (and also reversible) one-electron reduction process is observed at −2.56 V for **6**, consistent with yet another fullerene-based reduction step, which leads to formation of the hexaanion. Two additional reduction processes are observed at more negative potentials, which still appear to be at least partially reversible, but no attempt was made to measure their potentials accurately. The latter processes are centered around −3.3 V vs. Fc/Fc^+.

Figure 3. Cyclic voltammograms of compounds: a) **6** and b) **4**. Both were recorded under identical conditions with a scan rate of 100 mV/s. Internal ferrocene was added for potential reference in both cases, but is only shown for b)

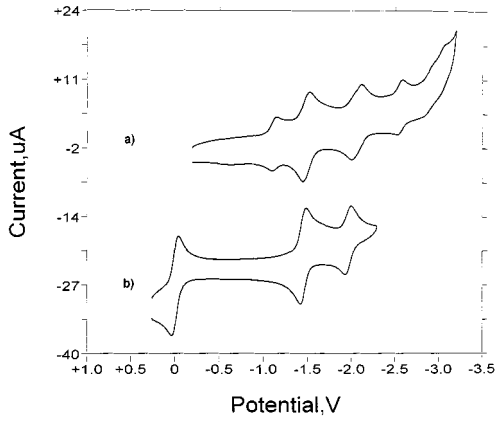

Figure 4 shows the cyclic voltammetric results obtained for compounds **5** and **7**. The first reduction process for **7** occurs at a relatively positive potential, −0.78 V (see Table 1), indicative of a process mostly localized on the very good acceptor adduct, the dicyano-*p*-quinonediimine (DCNQI). This is in accordance with recently reported results obtained for a similar compound.[31] This finding is further corroborated by the observation that this reduction potential is almost identical to the first reduction process observed for the model adduct, **5**, which occurs at −0.80 V. The second reduction process observed for **7** is broad and is clearly bigger than either the first one or any of the others, indicating that it probably corresponds to a two-electron process. It is centered around −1.13 V. This is very similar to the potential of −1.14 V measured for the second reduction of compound **5**. It is thus assigned to a two-electron reduction process, one component corresponding to the first fullerene-based reduction and the other to the formation of the dianion of the adduct. Thus, beyond this potential, the compound is found in its trianionic state at the electrode surface. The next reduction process observed for **7** has an $E_{1/2}$ of −1.52 V and, based on similar arguments as those outlined above in the case of **6**, can readily be as-

signed to the second fullerene-based reduction, for a total of 4 electrons per molecule, two in the adduct and two in the fullerene moiety. Two additional one-electron reduction processes are observed for **7**, one at −2.09 V and the other at −2.48 V, both of which must correspond to fullerene-based reductions. After these reductions, the compound is present as a hexaanionic species, with two electrons mainly localized on the DCNQI moiety and four on the fullerene group.

Figure 4. Cyclic voltammograms of compounds a) **7** and b) **5**, recorded under identical conditions with a scan rate of 100 mV/s. Internal ferrocene was added for potential reference in both cases, but is only shown for b)

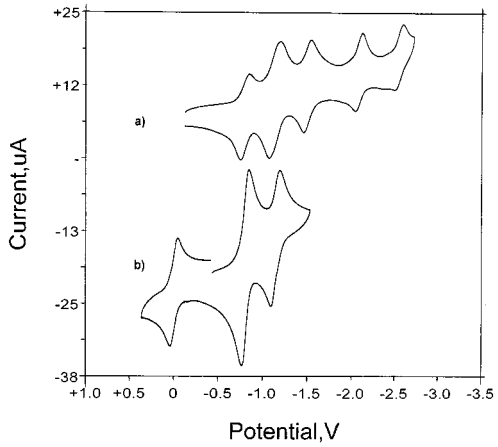

Cyclic voltammetric analysis of compound **8** shows four reversible reductions at −1.04, −1.44, −2.00, and −2.45 V (see Table 1) and one oxidation at +0.49 V. We believe that the four reductions are C_{60}-based. The oxidation wave is not reversible and its intensity seems smaller than those observed for the reduction waves during a cathodic scan. All evidence presently at hand seems to indicate that the compound decomposes following oxidation.

ESR Experiments: In order to obtain a direct measure of the extent of electron spin localization (or delocalization) for the different reduced states of the compounds studied here, samples were quantitatively electrolysed at controlled potential and then analysed by ESR spectroscopy. While a full interpretation of all the results has yet to be made, some striking observations are worthy of mention.

Figure 5 shows the ESR spectra of the monoanion radicals of compounds **5** and **7**, generated by controlled potential electrolysis under identical conditions as those described above for the electrochemical experiments. Figure 5c corresponds to the anion radical of the model compound **5** generated by potassium metal reduction in THF, which is presented for the sake of comparison. The important point to be noted from Figure 5 is the fact that the mono-reduced species of **7** shows an ESR spectrum which is very similar to that of **5**, with almost identical hyperfine patterns and *g* factors (**5** generated electrolytically in toluene/acetonitrile has a *g* factor of 2.00365, which compares well with the value of 2.00380 measured for $\mathbf{7}^-$). Small differences in resolution are attributed to ion pairing and electron-exchange differences.

Figure 6 shows a sequence of ESR spectra corresponding to the successive electrolytic reductions of **7**, starting with one electron and leading to four electrons (Figures 6a−6d, respectively). While the dianion signal is complex and is intermediate between those of the monoanion and the trianion, it may also contain additional features appropriate for a triplet state. Attempts to observe the half-field lines of a triplet state at 77 K met with failure, but further investigations are currently in progress. What is evident from Figure 6 is the fact that the first electron is essentially localized on the DCNQI moiety (g = 2.00380), while the third one is mainly localized on the fullerene nucleus (g = 2.00060). These observations are fully consistent with the observed voltammetric behavior, which suggests that the monoanion radical has the spin localized in the adduct, and that the trianion is a radical with two electrons paired in the adduct and an unpaired electron in the fullerene group. Interestingly, a fourth electron reduction, which presumably leads to the formation of a fullerene-based dianion, shows a strong ESR spectrum with very sharp resonances at a slightly larger *g* value. The precise origin of all of the observed spectral lines has yet to be fully delineated, although work in this area remains ongoing.

Figure 7 shows the sequence of ESR spectra for the successive electrolytic reductions of compound **6**, together with the ESR spectrum for the one-electron reduction product of the model compound **4**, shown as Figure 7f. Spectrum 7a, corresponding to the one-electron reduction species, clearly shows a fullerene-based signal, with a *g* factor of 2.00066. This ESR spectrum contains some additional spectral lines slightly downfield, which are typically observed for anions of fullerene derivatives, but have never been fully interpreted. The di-reduced species also appears to be fullerene-based, a fact impossible to assert from the voltammetric behavior, which showed two very close reductions at this potential. As a matter of fact, the controlled potential electrolysis process did not stop of its own accord as a consequence of the current decrease; it was manually stopped after the equivalent of charge corresponding to two electrons was reached. Note that this spectrum resembles the one shown in Figure 6d for compound **6**. This is reassuring since spectrum 6d was assigned to a species with two electrons in the fullerene, as is now being proposed for the dianion of **7**.

It is not until the third electron reduction of compound **6** (Figure 7c) that one begins to observe a clear resonance with the typical hyperfine pattern and the *g* factor of an anthraquinone-based spin system. However, the anthraquinone-based signal is rather small, and an additional broad resonance is observed between it and the fullerene-based signals. This broad resonance has not been definitively assigned, but it could arise as a consequence of another triple state. Addition of the fourth electron simply results in an enhanced signal for the anthraquinone-based resonance, with a concomitant decrease in the fullerene-based signals. Additionally, the broad intermediate signal is also enhanced

Figure 5. X-band ESR spectra for: a) electrolytically generated monoanion radical of **7**, in toluene/acetonitrile (85:15, v/v) containing 0.1 M $TBAPF_6$; b) electrolytically generated monoanion radical of **5** under identical solvent-electrolyte conditions; and c) potassium metal-reduced monoanion radical of **5** in THF, for comparison

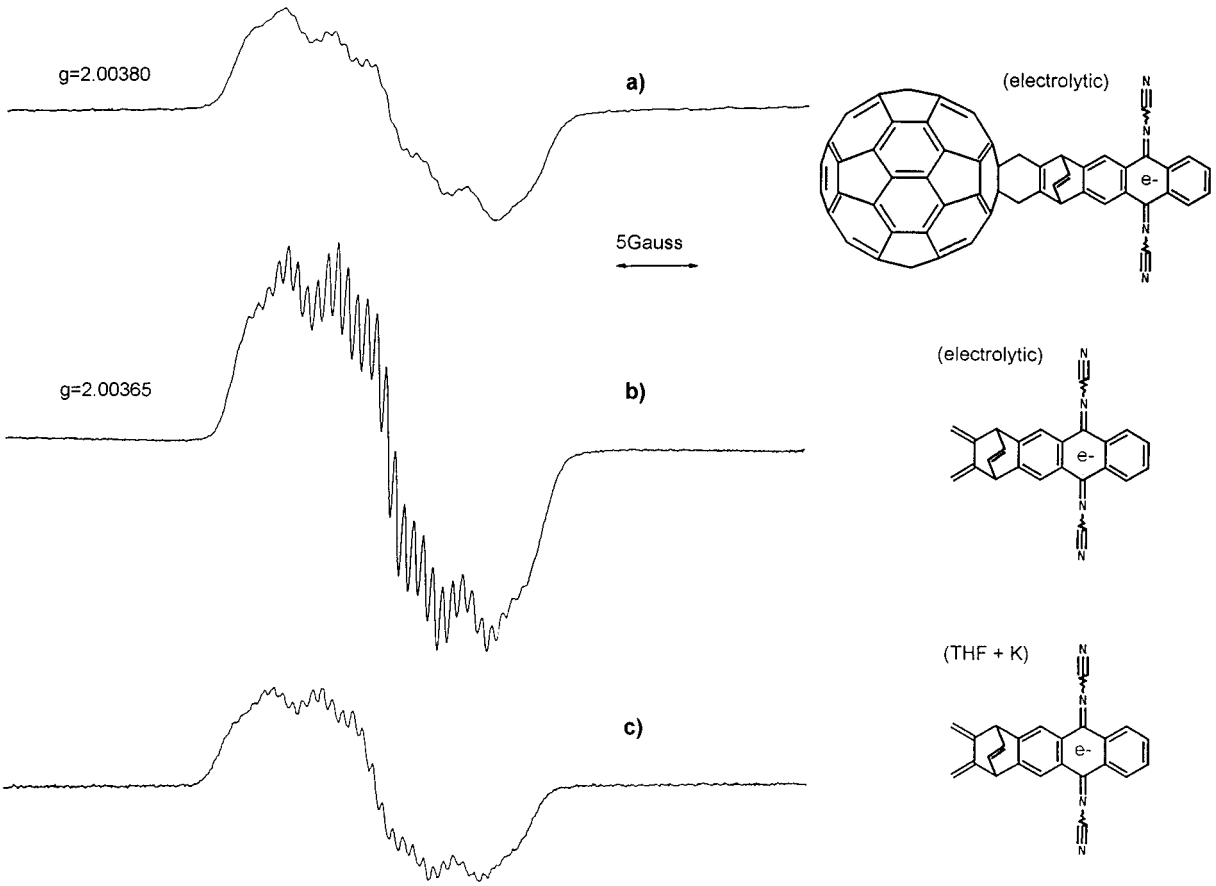

noticeably. The most striking (and unanticipated) result is observed after the fifth electron reduction, which clearly shows a single resonance based on the anthraquinone group. The *g* factor observed is 2.00469, which is very similar to the value of 2.00463 measured for the model anion radical ($\mathbf{4}^{-\cdot}$), see Figure 7f. This spectrum must then correspond to that of a pentaanionic species, which has four paired electrons in the fullerene group and a single unpaired electron in the anthraquinone adduct. The process was shown to be reversible by oxidative coulometry. This observation contradicts the expected behavior based on the voltammetric results. The latter predict that a pentaanion of **6** would have three fullerene-based electrons and two anthraquinone-based. Calculations are currently underway aimed at rationalizing these findings.

In order to further confirm the above observations, an experiment was conducted in THF, in which compound **6** was reduced with potassium metal in an all-glass apparatus under high vacuum conditions. The spectral sequence obtained is presented in Figure 8. While during the continuous alkali metal reduction it is not possible to know exactly the number of electrons corresponding to the various spectra, they were closely monitored after small incremental reductions were performed. We thus feel that we did not overlook any spectral intermediates in the sequence shown in Figure 8, which, upon inspection, clearly shows an almost identical sequence as that arising from the electrolytic experiment shown in Figure 7. The lack of resolution of the spectrum shown as Figure 8g was easily improved by lowering the temperature to −60°C, as shown in Figure 8h.

Computational Investigations: In order to ascertain whether the electrochemically determined locations of the first reduction or oxidation steps correspond to energy values and the coefficients of the frontier orbitals, we carried out a series of semiempirical calculations. The calculated structures of **6**–**8** (Figure 9) were obtained by PM3/RHF geometry minimization using the program package *HyperChem 5.0*.[45] In the case of **6** and **7,** the HOMOs are found to be fullerene-centered, since the orbital coefficients are almost exclusively localized on the C_{60} framework (Figures 9a,b). The calculated HOMO energies for **6** and **7** are −9.16 and −9.29 eV, respectively. The small energy difference is most likely attributable to the more pronounced $-I$ effect of the stronger DCNQI addend. As expected, the HOMO of the C_{60}-donor dyad **8** is addend-centered (Figure 8c), and the HOMO energy of −8.20 eV is significantly higher than that of **6** or **7**. In order to find out in which part of the dyads the first one-electron reduction takes place, we carried out PM3/UHF single-point calculations on the monoanions $\mathbf{6}^-$, $\mathbf{7}^-$ and $\mathbf{8}^-$ using the PM3/RHF geometries

Figure 6. X-band ESR spectra for the sequential electrolytic reduction of **7** in toluene/acetonitrile (85:15, v/v): a) after one-electron coulometric reduction, b) after two-electron reduction, c) after three-electron reduction, and d) after four-electron reduction

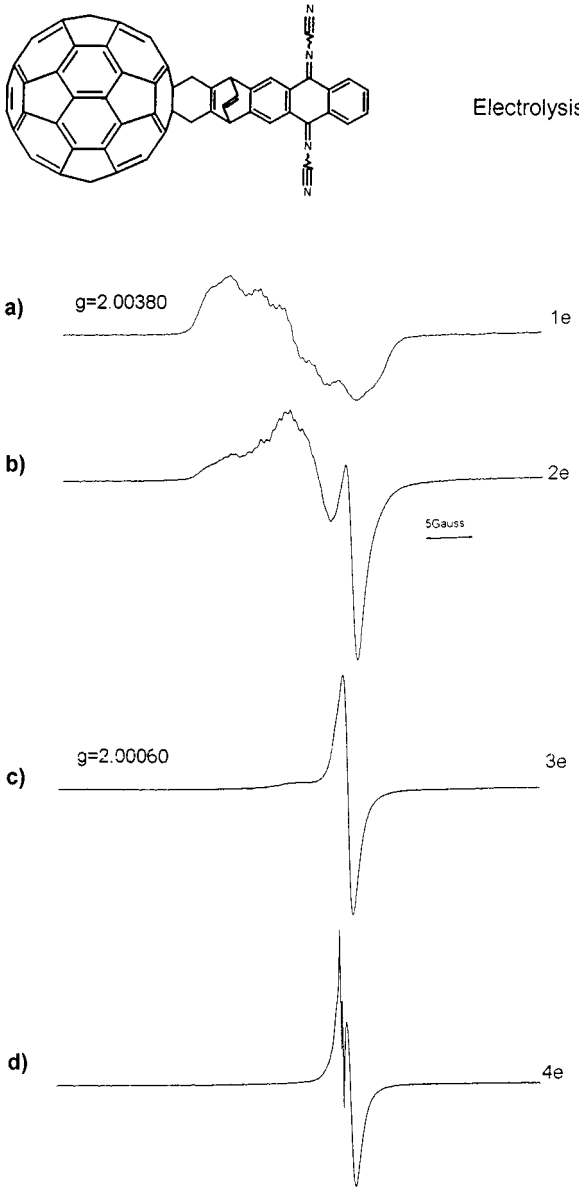

Figure 7. X-band ESR spectra for the sequential reduction of **6** in toluene/acetonitrile (85:15, v/v): a) after one-electron coulometric reduction, b) after two electrons, c) after three electrons, d) after four electrons, e) after five electrons; f) ESR spectrum for the monoanion radical of **4** generated by electrolytic reduction under identical conditions

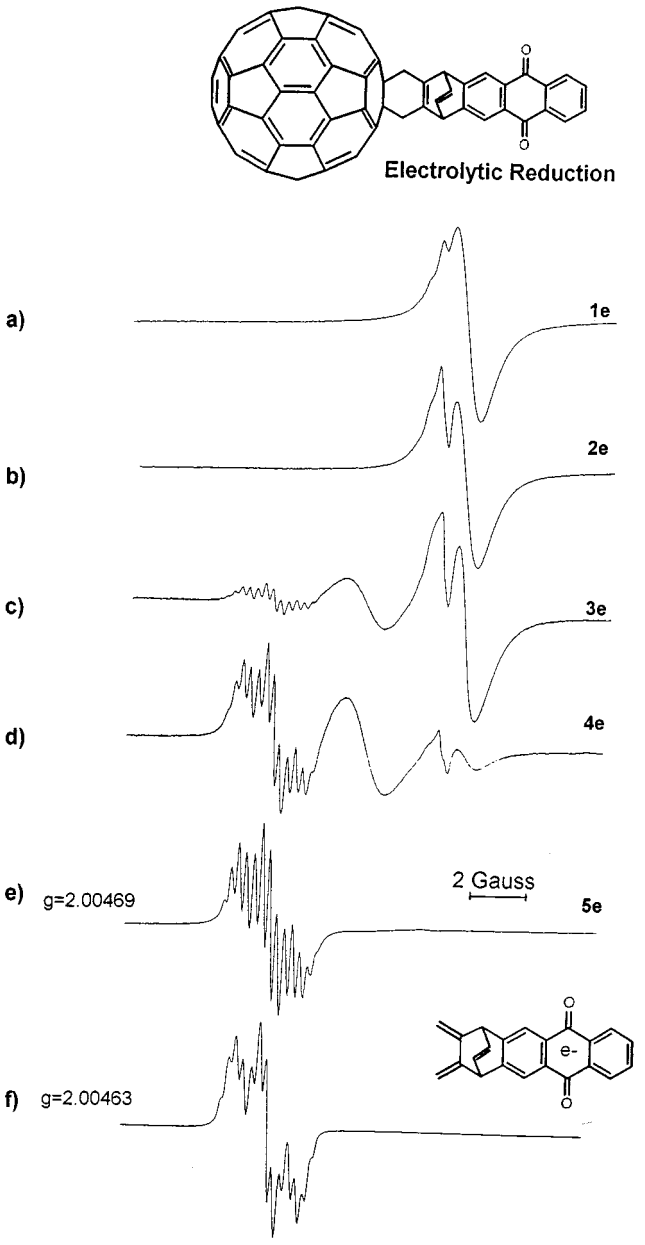

of **6**, **7** and **8**. This consideration of the SOMOs of the monoanions provides a more realistic estimation of reduction events than simply considering the LUMOs[32] of the neutral species. The latter qualitatively predicts the correct symmetry and coefficients of an unoccupied orbital. The order of orbital energies, however, might change if these states are filled with electrons.[46] The SOMO coefficients of $\mathbf{6}^-$ and $\mathbf{8}^-$ are predominantly located on the fullerene framework, whereas that of $\mathbf{7}^-$ is addend-centered (Figures 9d−f). Moreover, the SOMO energy of $\mathbf{7}^-$ (−3.51 eV) is lower than that of both $\mathbf{6}^-$ (−3.27 eV) and $\mathbf{8}^-$ (−3.19 eV). Hence, these calculations confirm the experimentally determined locations of the first one-electron reductions in the new dyads **6**−**8** and of the first oxidation in **8**. Calculations on more highly charged anions such as the pentaanion of **6** are more difficult to perform, since, for example, convergence problems arise. Moreover, the role of the counterions is expected to become increasingly important.

Summary and Conclusions: The synthesis of new C_{60}-acceptor dyads has been accomplished by facile and irreversible [4+2]cycloadditions of anthraquinone- and anthraquinodimethane-based dienes with C_{60}. On the other hand, a new C_{60}-donor system has been obtained by direct oxidative amination of C_{60} with *N,N′*-dimethyl-*o*-phenylenediamine.

Electrochemical reductions were shown to be highly localized, taking place either on the fullerene core or on the

Figure 8. Sequence of X-band ESR spectra for the continuous reduction of **6** with potassium in THF. From a) to g) the degree of reduction increases, but no exact number of electrons can be ascribed to each spectrum; h) corresponds to the same sample as in g) but recorded at −60°C to enhance its resolution. Note that this spectrum is very similar to that shown as Figure 7e

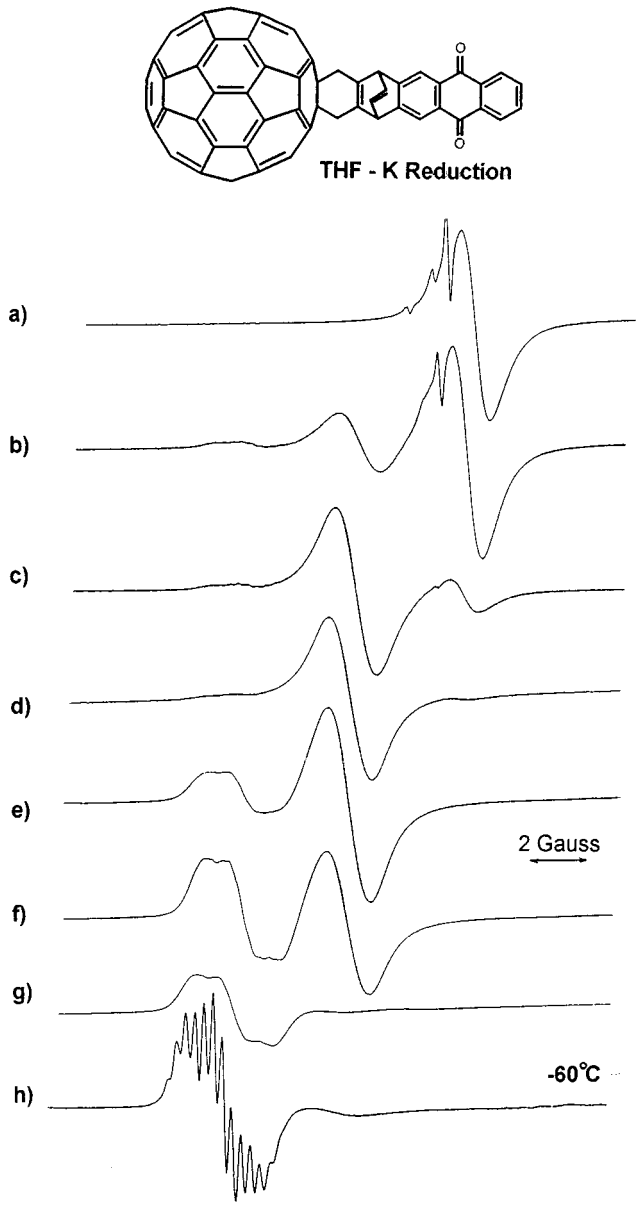

addend, depending on the relative electron affinities. In the case of **6**, the first reduction is fullerene-based, while for **7** it is addend-based. All other redox processes follow the expected order, with subsequent reductions of both the fullerene and the addend sometimes occurring almost simultaneously. ESR spectra are consistent with the electrochemical observations, with the exception of that for the pentaanion of **6**, which shows that spin localization occurs exclusively on the anthraquinone nucleus. This observation suggests that a diamagnetic tetraanion is present on the fullerene group and an unpaired spin is localized on the addend, contrary to the electrochemically predicted electron distribution with a fullerene trianion and a quinone dianion.

The electrochemical properties of the new dyads **6**–**8** have been rationalized on the basis of semiempirical PM3 calculations. The location of the first reduction or oxidation event correlates with the location of the HOMO coefficients of the neutral species or the SOMO coefficients of the monoanions. The reliability of such computational investigations should prove very useful for the systematic design of new dyads and triads involving the C_{60} building-block.

Figure 9. PM3-calculated frontier orbitals of **6**–**8** and their monoanions; a) HOMO of **6**, b) HOMO of **7**, c) HOMO of **8**, d) SOMO of $\mathbf{6}^-$, e) SOMO of $\mathbf{7}^-$ and f) SOMO of $\mathbf{8}^-$

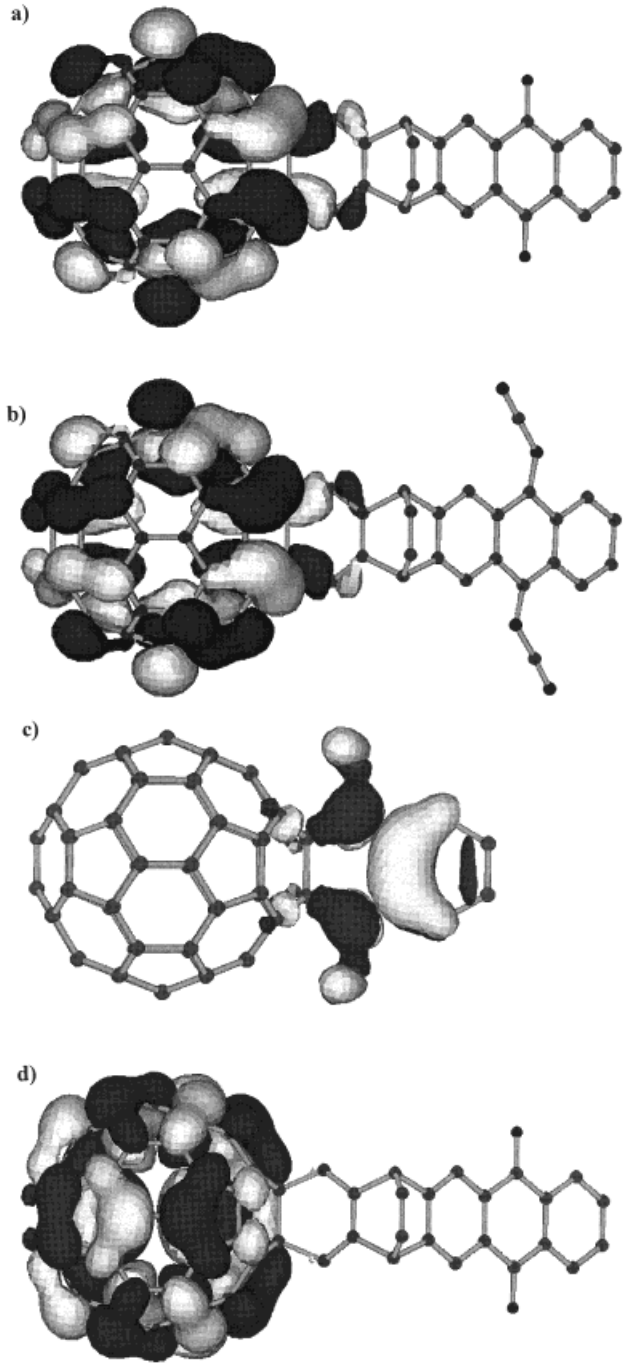

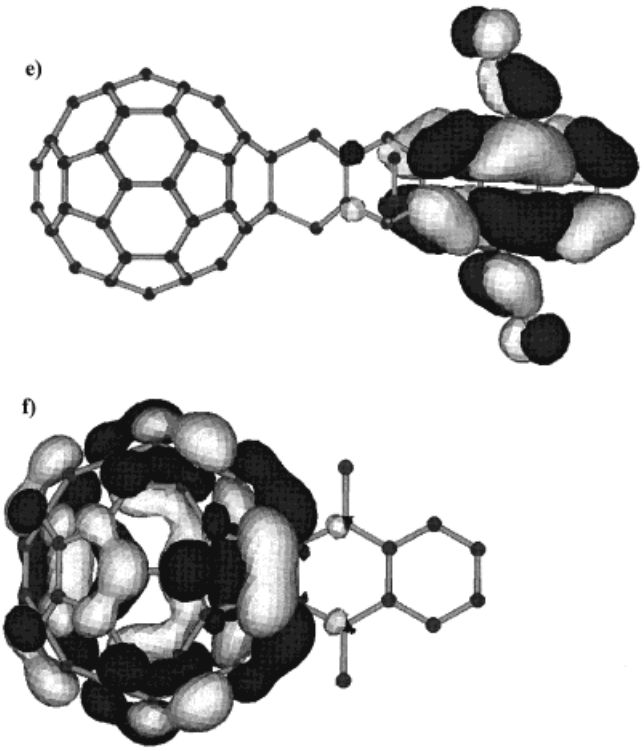

Whereas benzoquinone- or naphthoquinone-based addends are known to be stronger acceptors[32] than the fullerene, the anthraquinone moiety in **6** is a weaker acceptor than the C_{60} moiety. On the other hand, as shown by the example of the C_{60}-acceptor dyad **7**, the introduction of the more electron-withdrawing cyanoimino groups at the 9,10-positions of the anthracene unit causes the first reduction to take place on the addend. This experimental and computational study has shown that both the C_{60}-acceptor dyad **7** and the C_{60}-donor dyad **8** are suitable precursors for the synthesis of type-D triads (Figure 1). In these triads, which are bisadducts with respect to the fullerene core, C_{60} is expected to be a weaker acceptor compared to the situation in a monoadduct such as **6**–**8**. Investigations into the regioselective synthesis as well as the electrochemical and photophysical characterization of type-D triads with a stereochemically defined arrangement of the donor- and acceptor addend are currently in progress.

We gratefully acknowledge the generous financial support from the *NSF Chemistry Division* (CHE-9313018) to L. E. and from the *Bundesministerium für Bildung und Forschung* (BMBF) to A. H.

Experimental Section

Electrochemistry and ESR Experiments: Electrochemical measurements were made using a BAS 100W Electrochemical Analyzer (Bioanalytical Systems), and recorded using a Hewlett-Packard ColorPro plotter.[43] An electrochemical cell designed to carry out both cyclic voltammetry and bulk electrolysis under high-vacuum conditions was used.[44] For cyclic voltammetry, a glassy carbon working electrode (3 mm in diameter) was used after being polished with fraction one-quarter μm diamond polishing compound (Metadi II) from Buchler. A silver wire immersed in the solvent mixture containing the supporting electrolyte and separated from the bulk solution by a vycor tip served as a pseudo-reference electrode. The platinum wire used as the counterelectrode (1 mm diameter) was cleaned by heating in a flame for approximately 30 s. The supporting electrolyte, tetrabutylammonium hexafluorophosphate ($TBAPF_6$), was purchased from Fluka (>99%), recrystallized twice from an ethanol/water mixture (95:5), and dried in vacuo overnight prior to use.

All electrochemical experiments were carried out under the vapor pressure of the solvent system, after freezing in liquid nitrogen and evacuating to a pressure of about 10^{-5}–10^{-6} Torr for 4 h. Appropriate quantities of the supporting electrolyte and the fullerene (for typical concentrations of 0.1 M and 0.2 mM, respectively) were first placed in the electrochemical cell. Ferrocene was also added to the electrochemical cell as an internal reference (ferrocene/ferricinium, Fc/Fc^+) against which the potential values of all voltammetric waves were measured. The system was then evacuated to the pressures quoted above, and the solvent mixture (toluene/acetonitrile, 85:15) was vapor-transferred directly through the vacuum line. After the solvent had been transferred, the cell was removed from the vacuum line and the electrochemical experiment was allowed to proceed.

For bulk electrolysis, the working and the counterelectrodes consisted of Pt mesh and were separated by a fritted glass disk of low porosity (#4). The reference electrode was the same as that described for the voltammetric experiments. When ESR samples were needed, these were obtained in sealed 3-mm o.d. Pyrex tubes that were directly glassblown onto the electrochemical cell. After exhaustive electrolysis with the BAS 100W apparatus at the different potentials corresponding to the various anionic states, the cell was tilted in order to collect a sample in one of the tubes, which was then flame-sealed. The samples were analysed using the X-band of a Bruker ER 200 SRC ESR spectrometer equipped with a variable temperature facility.

General: ^1H NMR and ^{13}C NMR: JEOL PMX 60 and JEOL JNM GX 400. – MS: Varian MAT 311 A (EI) and Finnigan MAT 900 (FAB). – FT IR: Bruker Vector 22. – UV/Vis: Shimadzu UV 3102 PC. – TLC: Macherey-Nagel, Alugram Sil G/UV_{254}. Reagents used were commercially available reagent grade and were purified according to standard procedures. Products were isolated by flash column-chromatography (silica gel 60, particle size 0.04–0.063 mm).

1,4,4a,9a-Tetrahydro{[7,8-bis(methylene)]bicyclo[2.2.2]oct-2-eno}-[5,6-b]anthraquinone (**3**): A mixture of naphthoquinone (500 mg, 3.2 mmol) and the tetraene **2** (500 mg, 3.2 mmol) in toluene (100 ml) was heated under reflux for 2 h. The solvent was then evaporated under reduced pressure and the crude product was purified by recrystallization from chloroform/pentane to give 800 mg of the tetrahydroanthraquinone **3**. Yield: 80%. – ^1H NMR (400 MHz, $CDCl_3$, 25°C): δ = 2.39 (q, ^2J = 16.0 Hz , ^3J = 6.6 Hz, 2 H, aliph. CH_2), 2.63 (q, ^2J = 15.1 Hz, ^3J = 5.5 Hz, 2 H, alkyl CH_2), 3.35 (t, 2 H, CHCO), 3.83 (t, 2 H, bridgehead CH), 4.82 (s, 2 H, olef. CH_2), 5.07 (s, 2 H, olef. CH_2), 6.38 (t, 2 H, olef. CH), 7.72 (m, 2 H, arom. CH), 8.00 (m, 2 H, arom. CH). – ^{13}C NMR (100 MHz, $CDCl_3$, 25°C): δ = 26.06, 47.02, 52.58, 101.64, 126.82, 133.31, 133.89, 134.06, 134.20, 143.79, 197.63. – MS (EI): *m/z* = 314 [M^+], 155.– $C_{22}H_{18}O_2$: calcd. 314.1307, found 314.1300 (MS). – IR (KBr): ν = 3062, 2962, 2889, 2827, 1688, 1591, 1252, 879 cm^{-1}.

{[7,8-Bis(methylene)]bicyclo[2.2.2]oct-2-eno}-[5,6-b]-anthraquinone (**4**): To a suspension of tetrahydroanthraquinone **3** (800 mg, 2.55 mmol) in ethanol, a solution of KOH (710 mg, 12.7 mmol) in ethanol (10 ml) was added, while air was bubbled through

the solution. The mixture first turned red and then decolorized, whereupon the product was precipitated. The passage of air was maintained for a further 1 h. The crude product was then filtered off and washed with water, ethanol and diethyl ether. Further purification was achieved by flash chromatography (SiO_2/toluene) to give 600 mg of **4** as a yellow powder. Yield: 76%. − ^{1}H NMR (400 MHz, $CDCl_3$, 25°C): δ = 4.73 (t, 2 H, bridgehead C*H*), 5.11 (s, 2 H, olef. CH_2), 5.30 (s, 2 H, olef. CH_2), 6.65 (t, 2 H, olef. C*H*), 7.76 (m, 2 H, arom. C*H*), 8.13 (s, 2 H, arom. C*H*), 8.27 (m, 2 H, arom C*H*). − ^{13}C NMR (100 MHz, $CDCl_3$, 25°C): δ = 51.94, 105.84, 121.37, 127.10, 132.16, 133.52, 133.88 (2), 141.99, 148.46, 183.25. − MS (EI): *m/z* = 310 [M^+], 258, 91. − $C_{22}H_{14}O_2$: calcd. 310.0994, found 310.0998 (MS). − IR (KBr): ν = 3064, 2986, 1674, 1591, 1326, 1304, 1258, 960, 882, 711 cm^{-1}. − UV/Vis (CH_2Cl_2): λ_{max} (ε) = 272 (47000), 334 nm (4300).

N,N′-Dicyano{[7,8-bis(methylene)]bicyclo[2.2.2]oct-2-eno}-[5,6-b]-9,10-anthraquinonediimine (**5**): To a solution of anthraquinone **4** (154 mg, 0.5 mmol) in dichloromethane (15 ml), titanium tetrachloride (475 mg, 2.5 mmol) was added under nitrogen atmosphere, resulting in the formation of a yellow to brown precipitate. Subsequently, bis(trimethylsilyl)carbodiimide (1.16 g, 5 mmol) was added, which caused the precipitate to dissolve and the reaction mixture to darken. The solution was stirred at room temperature overnight, while the progress of the reaction was monitored by TLC. After 24 h, the mixture was treated with ice-water (25 ml). The organic layer was diluted with dichloromethane until a clear solution was formed and then the phases were separated. After drying the organic phase with magnesium sulfate, the solvent was evaporated under reduced pressure. Further purification by flash chromatography (SiO_2, dichloromethane) afforded 90 mg of **5** as an orange powder. Yield: 50%. − ^{1}H NMR (400 MHz, $CDCl_3$, 25°C): δ = 4.76 (t, 2 H, bridgehead C*H*), 5.14 (s, 2 H, olef. CH_2), 5.32 (s, 2 H, olef. CH_2), 6.65 (t, 2 H, olef. C*H*), 7.83 (s, 2 H, arom. C*H*), 8.69 (br. s, 4 H, arom. C*H*). − ^{13}C NMR (100 MHz, $CDCl_3$, 25°C): δ = 51.82, 106.52, 113.83, 121.72, 127.52, 133.67, 134.51, 141.11, 149.48, 171.60. − MS (EI): *m/z* = 358 [M^+], 306. − $C_{24}H_{14}N_4$: calcd. 358.1218, found 358.1215 (MS). − IR (KBr): ν = 3074, 3062, 2984, 2925, 2161, 1562, 1334, 897, 685 cm^{-1}. − UV/Vis (CH_2Cl_2): λ_{max} (ε) = 226 (62000), 280 (58000), 347 nm (37000).

Compound **6**: A mixture of C_{60} (100 mg, 0.14 mmol) and anthraquinone **4** (43 mg, 0.14 mmol) in toluene (100 ml) was heated to reflux for 3 h under a nitrogen atmosphere. The progress of the reaction was monitored by TLC (toluene). Subsequently, the solution was concentrated under reduced pressure to a volume of ca. 50 ml. Flash chromatography (SiO_2, toluene) furnished 70 mg of the monoadduct **6**. Yield: 49%. − ^{1}H NMR (400 MHz, $CDCl_3$, 25°C): δ = 4.31 (q, 4 H, CH_2), 5.45 (t, 2 H, bridgehead C*H*), 7.26 (m, 2 H, olef. C*H*), 7.75 (m, 2 H, arom. C*H*), 8.13 (s, 2 H, arom. C*H*), 8.24 (m, 2 H, arom. C*H*). − ^{13}C NMR (100 MHz, $CDCl_3$, 25°C): δ = 44.39, 53.65, 66.95, 120.68, 127.04, 129.03, 130.84, 133.84, 135.32, 135.68, 139.12, 139.96, 140.09, 141.44, 141.55, 141.68, 142.02, 142.26, 142.52, 142.86, 143.08, 144.60, 144.67, 144.93, 145.28, 145.40, 145.44, 145.51, 145.60, 145.77, 146.15, 146.21, 146.39, 146.50, 147.50, 153.97, 156.36, 157.06, 183.40. − MS (MALDI-TOF): *m/z* = 1047 [M^+ + OH], 1029 [M^+ − H]. − IR (KBr): ν = 3065, 2923, 1667, 1590, 1427, 1323, 1298, 953, 714, 527 cm^{-1}. − UV/Vis (CH_2Cl_2): λ_{max} (ε) = 256 (149000), 312 (57000), 434 (5100), 547 (1350), 704 nm (490).

Compound **7**: A mixture of C_{60} (100 mg, 0.14 mmol) and dicyanoanthraquinonediimine **5** (50 mg, 0.14 mmol) in toluene (100 ml) was heated to reflux for 3 h under a nitrogen atmosphere. The progress of the reaction was monitored by TLC (toluene/AcOEt, 98:2). The solvent was then evaporated under reduced pressure until a volume of ca. 50 ml remained. Flash chromatography (SiO_2, toluene/AcOEt, 98:2) furnished 60 mg of the monoadduct **7**. Yield 42%. − ^{1}H NMR (400 MHz, $CDCl_3$, 25°C): δ = 4.33 (q, 4 H, CH_2), 5.47 (s, 2 H, bridgehead C*H*), 7.28 (t, 2 H, olef. C*H*), 7.77 (s, 2 H, arom. C*H*), 8.5 (br. s, 4 H, arom. C*H*). − ^{13}C NMR (100 MHz, $CDCl_3$, 25°C): δ = 44.66, 53.65, 67.17, 113.85, 121.54, 127.30, 134.33, 135.02, 135.65, 138.31. 140.00, 140.21, 140.94, 141.38, 141.57, 141.88, 142.06, 142.20, 142.52, 143.12, 144.45, 144.51, 144.65, 144.73, 145.24, 145.28, 145.35, 145.42, 145.51, 145.71, 146.15, 146.21, 146.30, 146.54, 147.61, 148.12, 156.07, 156.49, 172.24. − MS (FAB): *m/z* = 1080 [M^+ + H], 720. − IR (KBr): ν = 3072, 2952, 2922, 2867, 2160, 1560, 1427, 1330, 767, 689, 527 cm^{-1}. − UV/Vis (CH_2Cl_2): λ_{max} (ε) = 255 (92000), 317 (49000), 434 (4400), 706 nm (190).

Compound **8**: A mixture of C_{60} (500 mg, 0.69 mmol) and *N,N′*-dimethyl-*o*-phenylenediamine (2.0 g, 14.7 mmol) in toluene (500 ml) was heated at 90°C for 14 d. The progress of the reaction was monitored by TLC (toluene/cyclohexane, 2:1). The product was subsequently isolated by flash chromatography (SiO_2, toluene/cyclohexane, 2:1) in the form of brown microcrystals (120 mg). Yield 20%. − ^{1}H NMR (400 MHz, $CDCl_3$, 25°C): δ = 3.78 (s, 6 H, CH_3), 7.17 (s, 4 H, arom. C*H*). − ^{13}C NMR (100 MHz, $CDCl_3$, 25°C): δ = 37.28, 86.02, 115.37, 122.42, 136.65, 138.28, 141.20, 141.60, 141.71, 142.04, 142.42, 142.75, 144.40, 144.91, 145.28, 145.60, 145.86, 146.35, 147.81, 148.84. − MS (FAB): *m/z* = 854 [M^+], 720. − IR (KBr): ν = 3057, 2953, 2851, 2797, 1593, 1498, 1462, 1446, 1293, 1178, 1130, 1108, 952, 910, 739, 526 cm^{-1}. − UV/Vis (CH_2Cl_2): λ_{max} (ε) = 255 (178000), 314 (56000), 532 (1900), 689 nm (540).

[1] A. Hirsch, *The Chemistry of the Fullerenes*, Georg Thieme, Stuttgart, **1994**.
[2] A. Hirsch, *Synthesis* **1995**, 895.
[3] F. Diederich, C. Thilgen, *Science* **1996**, *271*, 317.
[4] Q. Xie, E. Perez-Cordero, L. Echegoyen, *J. Am. Chem. Soc*. **1992**, *114*, 3978.
[5] H. Imahori, Y. Sakata, *Adv. Mat*. **1997**, *9*, 537.
[6] D. Gust, T. A. Moore, A. L. Moore, *Res. Chem. Intermed*. **1997**, *23*, 621.
[7] P. A. Liddell, J. P. Sumida, A. N. Macpherson, L. Noss, G. R. Seely, K. N. Clark, A. L. Moore, T. A. Moore, D. Gust, *Photochem. Photobiol*. **1994**, *60*, 537.
[8] T. Drovetskaya, C. A. Reed, P. Boyd, *Tetrahedron Lett*. **1995**, *36*, 7971.
[9] H. Imahori, Y. Sakata, *Chem. Lett*. **1996**, 199.
[10] H. Imahori, K. Hagiwara, M. Aoki, T. Akiyama, S. Taniguchi, T. Okada, M. Shirakawa, Y. Sakata, *J. Am. Chem. Soc*. **1996**, *118*, 11771.
[11] M. G. Ranasinghe, A. M. Oliver, D. F. Rothenfluh, A. Salek, M. N. Paddon-Row, *Tetrahedron Lett*. **1996**, *37*, 4797.
[12] P. S. Baran, R. R. Monaco, A. U. Khan, D. I. Schuster, S. R. Wilson, *J. Am. Chem. Soc*. **1997**, *119*, 8363.
[13] R. M. Williams, J. M. Zwier, J. W. Verheuven, *J. Am. Chem. Soc*. **1995**, *117*, 4093.
[14] J. M. Lawson, A. M. Oliver, D. F. Rothenfluh, Y. An, G. A. Ellis, M. G. Ranasinghe, S. I. Khan, A. G. Franz, P. S. Ganapathi, M. J. Shephard, M. N. Paddon-Row, Y. Rubin, *J. Org. Chem*. **1996**, *61*, 5032.
[15] R. M. Williams, M. Koeberg, J. M. Lawson, Y. An, Y. Rubin, M. N. Paddon-Row, J. W. Verheuven, *J. Org. Chem*. **1996**, *61*, 5055.
[16] Y. Nakamura, T. Minowa, S. Tobita, H. Shizuka, J. Nishimura, *J. Chem. Soc., Perkin Trans. 2,* **1995**, 2351.
[17] G. Torres-Garcia, H. Luftmann, C. Wolff, J. Mattay, *J. Org. Chem*. **1997**, *62*, 2752.
[18] N. S. Sariciftci, F. Wudl, A. J. Heeger, M. Maggini, G. Scorrano, M. Prato, J. Bourassa, P. C. Ford, *Chem. Phys. Lett*. **1995**, *247*, 510.
[19] H. Imahori, S. Cardoso, D. Tatman, S. Lin, L. Noss, G. R.

Seely, L. Sereno, J. C. de Silber, T. A. Moore, A. L. Moore, D. Gust, *Photochem. Photobiol*. **1995**, *62*, 1009.
[20] M. Maggini, A. Karlsson, G. Scorrano, G. Sandona, G. Farnia, M. Prato, *J. Chem. Soc., Chem. Commun*. **1994**, 589.
[21] D. M. Guldi, M. Maggini, G. Scorrano, M. Prato, *J. Am. Chem. Soc*. **1997**, *119*, 974.
[22] D. M. Guldi, M. Maggini, G. Scorrano, M. Prato, *Res. Chem. Intermed*. **1997**, *23*, 561.
[23] T. G. Linssen, K. Dürr, M. Hanack, A. Hirsch, *J. Chem. Soc., Chem. Commun*. **1995**, 103.
[24] K. Dürr, S. Fiedler, T. Linssen, A. Hirsch, M. Hanack, *Chem. Ber.* **1997**, *130*, 1375.
[25] N. Martin, I. Perez, L. Sanchez, C. Seoane, *J. Org. Chem*. **1997**, *62*, 5690.
[26] M. Iyoda, F. Sultana, S. Sasaki, M. Yoshida, *J. Chem. Soc., Chem. Commun*. **1994**, 1929.
[27] W. Bidell, R. E. Douthwaite, M. L. H. Green, A. H. H. Stephens, J. F. C. Turner, *J. Chem. Soc., Chem. Commun.* **1994**, 1641.
[28] M. Iyoda, S. Sasaki, F. Sultana, M. Yoshida, Y. Kuwatani, S. Nagase, *Tetrahedron Lett*. **1996**, *37*, 7987.
[29] M. Iyoda, F. Sultana, A. Kato, M. Yoshida, Y. Kuwatani, M. Komatsu, S. Nagase, *Chem. Lett*. **1997**, 63.
[30] T. Ohno, N. Martin, B. Knight, F. Wudl, T. Suzuki, H. Yu, *J. Org. Chem*. **1996**, *61*, 1306.
[31] B. Illescas, N. Martin, C. Seoane, *Tetrahedron Lett*. **1997**, *38*, 2015.
[32] B. M. Illescas, N. Martin, C. Seoane, E. Orti, P. M. Viruela, R. Viruela, A. de la Hoz, *J. Org. Chem*. **1997**, *62*, 7585.
[33] P. A. Liddell, D. Kuciauskas, J. P. Sumida, B. Nash, D. Nguyen, A. L. Moore, T. A. Moore, D. Gust, *J. Am. Chem. Soc*. **1997**, *119*, 1405.
[34] [34a] A. Hirsch, I. Lamparth, H. R. Karfunkel, *Angew. Chem.* **1994**, *106*, 453; *Angew. Chem. Int. Ed. Engl*. **1994**, *33*, 437. – [34b] A. Hirsch, I. Lamparth, T. Grösser, H. R. Karfunkel, *J. Am. Chem. Soc.* **1994**, *116*, 9385. – [34c] I. Lamparth, C. Maichle-Mössmer, A. Hirsch, *Angew. Chem.* **1995**, *107*, 1755; *Angew. Chem. Int. Ed. Engl*. **1995**, *34*, 1607. – [34d] I. Lamparth, A. Herzog, A. Hirsch, *Tetrahedron* **1996**, *52*, 5065. – [34e] F. Djojo, A. Herzog, I. Lamparth, F. Hampel, A. Hirsch, *Chem. Eur. J.* **1996**, *2,* 1537. – [34f] X. Camps, H. Schönberger, A. Hirsch, *Chem. Eur. J.* **1997**, *3*, 561.
[35] A. Aumüller, S. Hünig, *Liebigs Ann. Chem*. **1986**, 142.
[36] A. Aumüller, S. Hünig, *Liebigs Ann. Chem*. **1986**, 165.
[37] A. Chollet, M. Wismer, P. Vogel, *Tetrahedron Lett*. **1976**, *47*, 4271.
[38] R. Gabioud, P. Vogel, *Tetrahedron* **1980**, *36*, 149.
[39] W. Lehnert, *Tetrahedron Lett*. **1970**, 4723.
[40] [40a] K.-D. Kampe, N. Egger, M. Vogel, *Angew. Chem*. **1993**, *105*, 1203; *Angew. Chem. Int. Ed. Engl*. **1993**, *32*, 1174. – [40b] G. Schick, K. D. Kampe, A. Hirsch, *J. Chem. Soc., Chem. Commun.* **1995**, 2289.
[41] G. W. H. Cheeseman, *J. Chem. Soc*. **1955**, 3308.
[42] F. Arias, L. Echegoyen, S. R. Wilson, Q. Lu, Q. Lu, *J. Am. Chem. Soc.* **1995**, *117*, 1422.
[43] Y. Yang, F. Arias, L. Echegoyen, L. P. F. Chibante, S. Flanagan, A. Robertson, L. Wilson, *J. Am. Chem. Soc.* **1995**, *117*, 7801.
[44] M. Delgado, D. A. Gustowski, H. K. Yoo, G. W. Gokel, L. Echegoyen, *J. Am. Chem. Soc.* **1988**, *110*, 119.
[45] *HyperChem 5.0*, Hypercube, Inc., Waterloo, Ontario N2L 2X2, Canada **1997**.
[46] A change in the order of orbital energies is seen, for example, by comparing **7** with $\mathbf{7}^-$. Whereas the LUMO of **7** is fullerene-centered, the SOMO of $\mathbf{7}^-$ is addend-centered.

[97385]